ARCHIVES OF ACOUSTICS
18, 1, 131–156 (1993)

EXPERIMENTAL INVESTIGATION OF DISCRETE SOUND PRODUCTION IN DEEP CAVITY EXPOSED TO AIRFLOW

M. MEISSNER

Institute of Fundamental Technological Research
Polish Academy of Sciences
(00-049 Warszawa, ul. Świętokrzyska 21)

The results are presented of the experimental investigation of the discrete sound generation in the process of airflow over the deep cavity. During the increase of the airflow velocity, three discrete components, referred to as A, B and C, are excited successively, which, as indicated by a analysis of results, are the f_{13}, f_{12} and f_{11} modes, respectively. In the process of sound generation two stages have been distinguished: stage 1, characterized by strong dependence of the frequencies of the discrete components A, B and C on the velocity of the airflow and stage 2, where the frequency, of the discrete component C, as the function of the velocity, varies approximately ten times less as compared with the stage 1. In stage 1 the "leading edge — trailing edge interaction" is of fundamental significance in the production of the discrete components, whereas the stage 2 is dominated by the feedback involving the effect of cavity-resonance modes on the disturbances of the shear layer.

1. Introduction

Frequently the airflow over a cavity is accompanied by generation of discrete sound, i.e. the acoustic signal consisting of discrete frequency components. This feature, exploited in musical instruments [1–3], is undesirable in wind tunnels with slotted walls [4, 5], in the industrial flow installations [6] and during the motion of various objects (aircraft, for example) in a static medium [7, 8] (detailed discussion of the sound generation phenomenon during flow over cavities can be found in review articles [9, 10]). So far, main research effort was placed on understanding the mechanism of the discrete sound generation and the role of the cavity in this process (shallow cavity [11–14], deep cavity [15–22], the cavity in the form of a Helmholtz resonator [23–27]) as well as the flow structure (laminar or turbulent flow [21, 28]). In case of the airflow over a deep cavity the experimental studies [19, 20] revealed the occurrence of the three different kinds of discrete components: pipetones, sheartones and turbulence-generated tones; the latter constitute a "passive response of cavity" to the turbulences in the airflow. The mechanism of pipetones generation, analogous to the process in organ pipes, is based on the mutual interactions between shear layer disturbances and cavity-resonance modes. In the process of the sheartone generation, the basic is the "leading edge — trailing edge interaction", i.e. the effect of the acoustic perturbations occurring at the leading edge, on the shear

layer disturbances at the trailing edge. Similar mechanism produces discrete sound when the air stream flows over shallow cavities [7, 11, 13] and also in generating edge-tones [29–31], where jumps in frequency of tones and hysteresis are observed.

This study presents the experimental results of generation of the discrete sound by the airflow over the deep cavity with rectangular opening. In the experimental setup, planar jet was used to excite oscillations in the cavity, in contrast to the methods used by other authors. The aim of this study is to identify the mechanism of discrete component generation.

2. Experimental arrangement and apparatus

The experimental setup is shown in Fig. 1a. The main components of the system are:

a) inlet nozzle *1* of circular cross-section,

b) settling chamber *2*,

c) preliminary nozzle *3*, of 3 × 30 mm cross-section and 60 mm length,

d) nozzle head *4*, with outlet nozzle and cavity opening: dimensions are l = 8 mm, s = 28 mm and thickness d_0 = 2 mm (Fig. 1b).

e) cavity *5* with s = 28 mm, w = 40 mm and depth d: 12 cm, 14 cm, 16 cm and 18 cm, respectively.

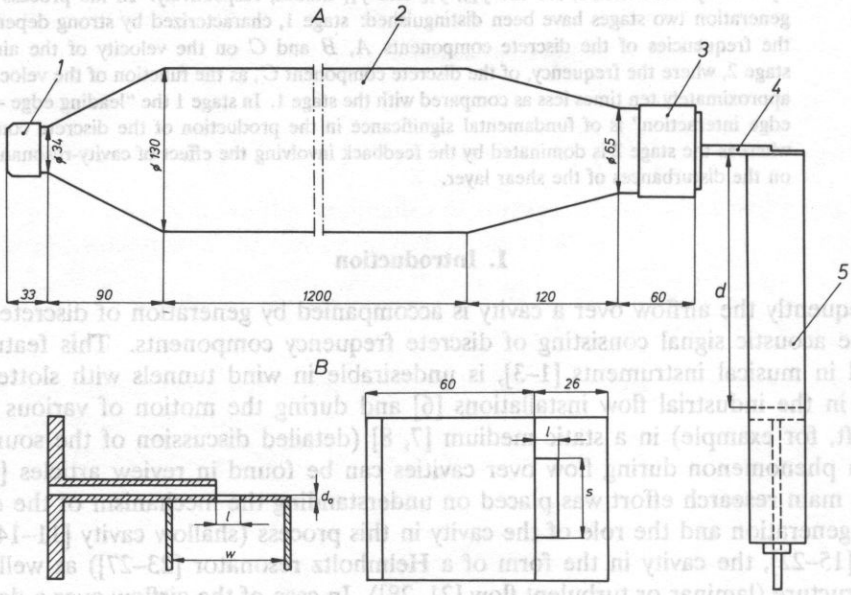

FIG. 1. Experimental setup: a) general layout, b) outlet attachment.
1 — inlet nozzle, *2* — settling chamber, *3* — preliminary nozzle, *4* — nozzle head, *5* — cavity.

The measuring system was supplied with the compressed air at the max. pressure 0.5 MPa. The air was fed through the control valve to the settling chamber *2*, and subsequently exited via the nozzle *3* and head *4*. The flow rate, in m^3/s, was measured with model PG 08–704 rotameter made by Prüfgerate-Werk Medingen. Acoustic measurements were

made with Brüel and Kjaer instrumental setup consisting of the microphone 1" type 4145, preamplifier 2203 and narrowband spectrum analyser 2033. All the measurements were conducted in an anechoic room. The microphone was mounted at the distance 1.5 m from the cavity opening: the line joining the centre of the microphone and the centre of the orifice made 90° angle with the air stream axis and crossed the plane of the orifice at 30°. The experiments contained the following:

a) measurement of the frequency f and the acoustic pressure level P of the discrete components at the low stream velocities,

b) recording of the selected sound spectra.

With the spectrum analyser 2033 the frequency analysis of the signal can be made within the defined frequency range. The accuracy of the frequency measurement is the same at a given frequency range. For the cavity depths equal 12 cm, 14 cm, 16 cm and 18 cm, the frequency range was up to 1000 Hz, with the accuracy of the frequency readout 2.5 Hz, for the first two and up to 500 Hz for the remaining two, accurate to 1.25 Hz. The acoustic pressure level P has been measured with the accuracy 0.1 dB in the whole frequency range. Choosing one of the modes of 2033 spectrum analyser, with 16–samples linear averaging, it was possible to eliminate the errors due to fluctuations of the main flow.

The selected sound spectra have been recorded with the data analysis system providing for the screen-copy of 2033 analyser. The system consists of an IBM XT computer as a control unit, IEC 625 interface, the spectrum analyser 2033 and Star SG–10 printer.

3. Sound spectra

In Figs. 2, 3 the sound spectra are shown, obtained at one of the four cavity depths (d = 12 cm) at the different values of the average stream velocities U (U = flow rate per outlet nozzle area). As follows from Figs. 2a, b, c the first discrete component (A — component) in the sound spectrum arises at the flow velocity U of order of a few m/s. This component is almost monochromatic and at relatively high acoustic pressure level ($P \leq 49$ dB) can easily be distinguished against broadband noise. Strong dependence of A–component frequency is observed on the airflow velocity. At U = 4.75 m/s (P–maximum of A–component) the frequency is 512.5 Hz (Fig. 2a), whereas at the velocities U: 5.16 m/s and 5.57 m/s the frequencies are 535 Hz (Fig. 2b) and 560 Hz (Fig. 2c), respectively. At the velocity U = 6.05 m/s (Fig. 2d) the first qualitative change takes place in the observed phenomenon: the discrete component A disappears and the second discrete component, referred to as component B, arises in the sound spectrum. It follows from Figs. 2c, 2d, that the component B maintains the tonal character but its frequency at U = 6.05 m/s (f = 492.5 Hz) is much lower than that of component A at U = 5.57 m/s. Further increase of U effects a fast increase of B–component frequency. In the case of the maximum of P for this component, the frequency amounts to 505 Hz (Fig. 2e) which, as one can see comparing Fig. 2a, approaches the frequency of component A at its value of the maximum P. At the velocity U = 6.48 m/s (Fig. 2f) another qualitative change is observed in the phenomenon: the discrete component B vanishes and the third discrete component (component C) in the sound spectrum occurs. It follows from Figs. 2e, 2f that, in the velocity range 6.28–6.48 m/s, consecutive, sudden drops in the frequency of the generated sound, take place.

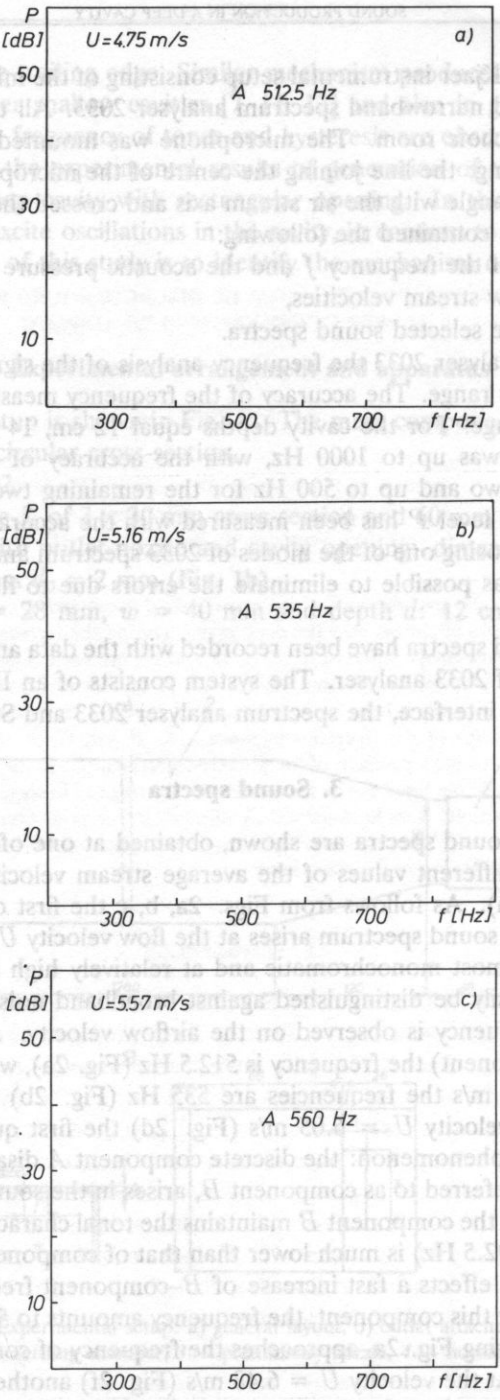

FIG. 2. Sound spectra at the flow velocities U: a) 4.75 m/s, b) 5.16 m/s, c) 5.57 m/s,

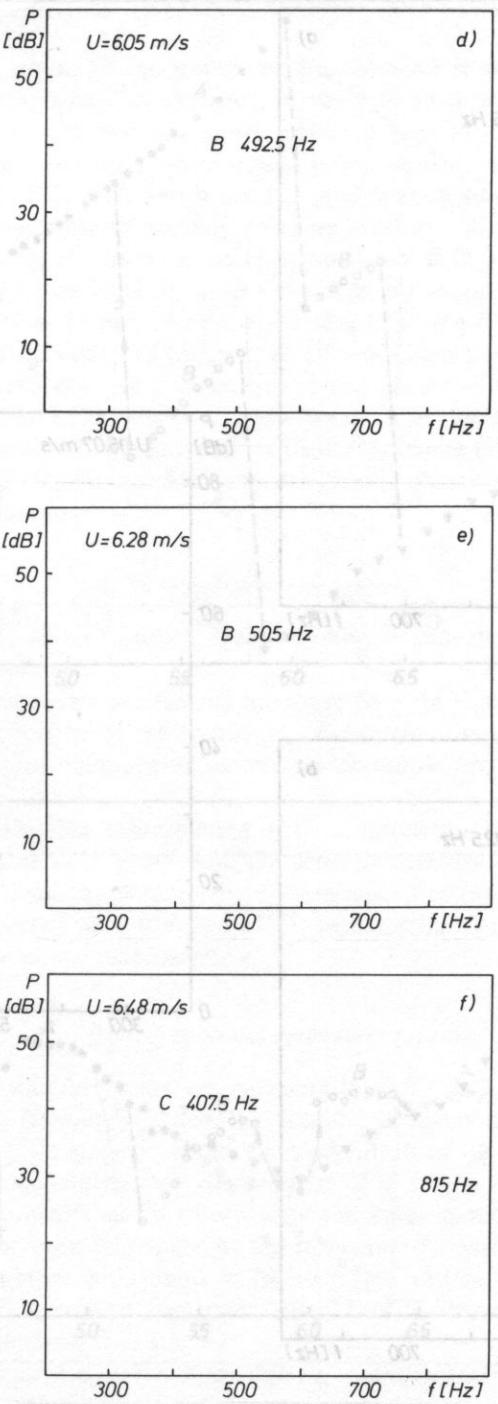

FIG. 2. Sound spectra at the flow velocities U: d) 6.05 m/s, e) 6.28 m/s, f) 6.48 m/s. Cavity depth $d = 12$ cm.

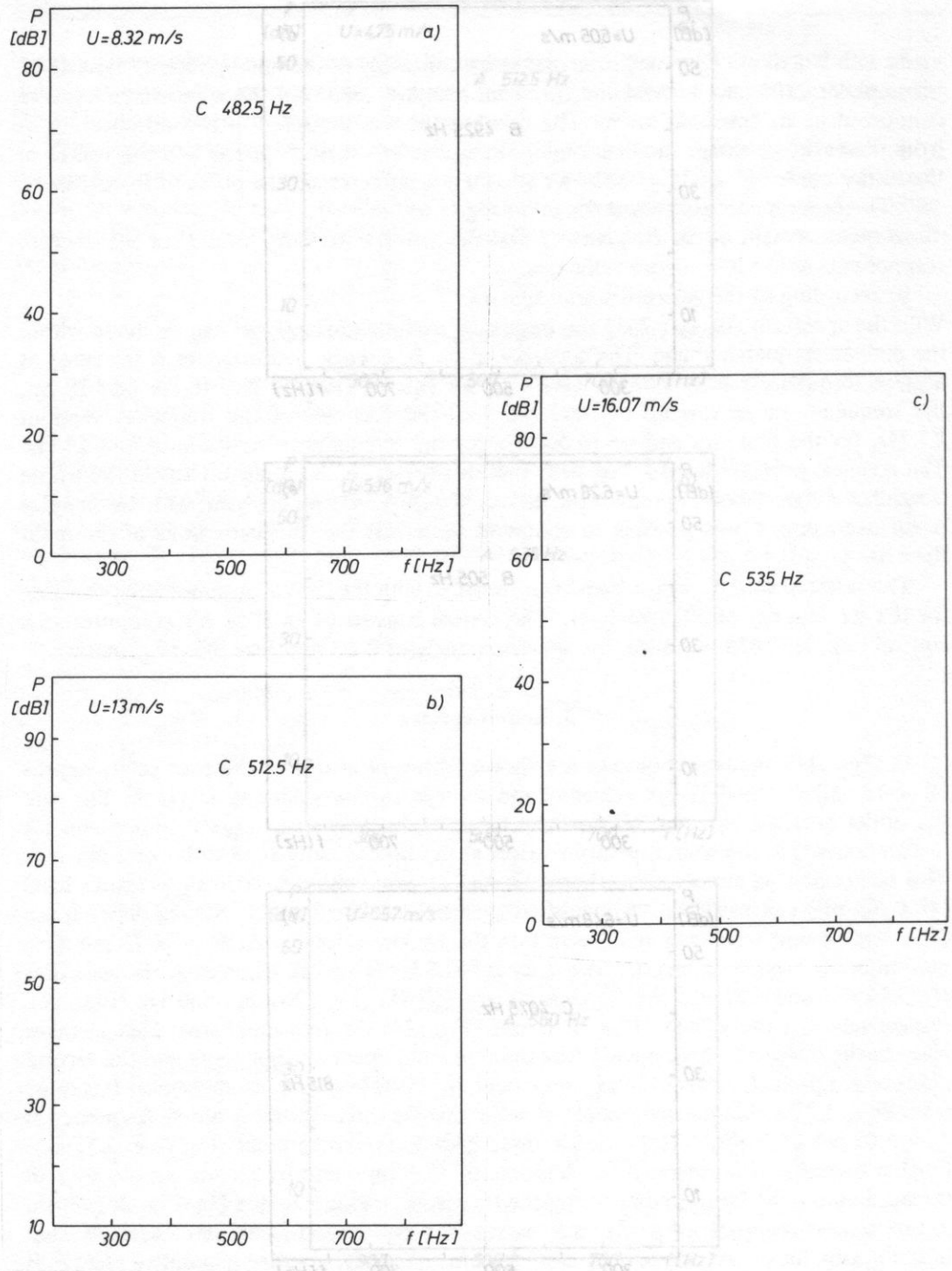

FIG. 3. Sound spectra at the flow velocities U: a) 8.32 m/s, b) 13 m/s, c) 16.07 m/s. Cavity depth d = 12 cm.

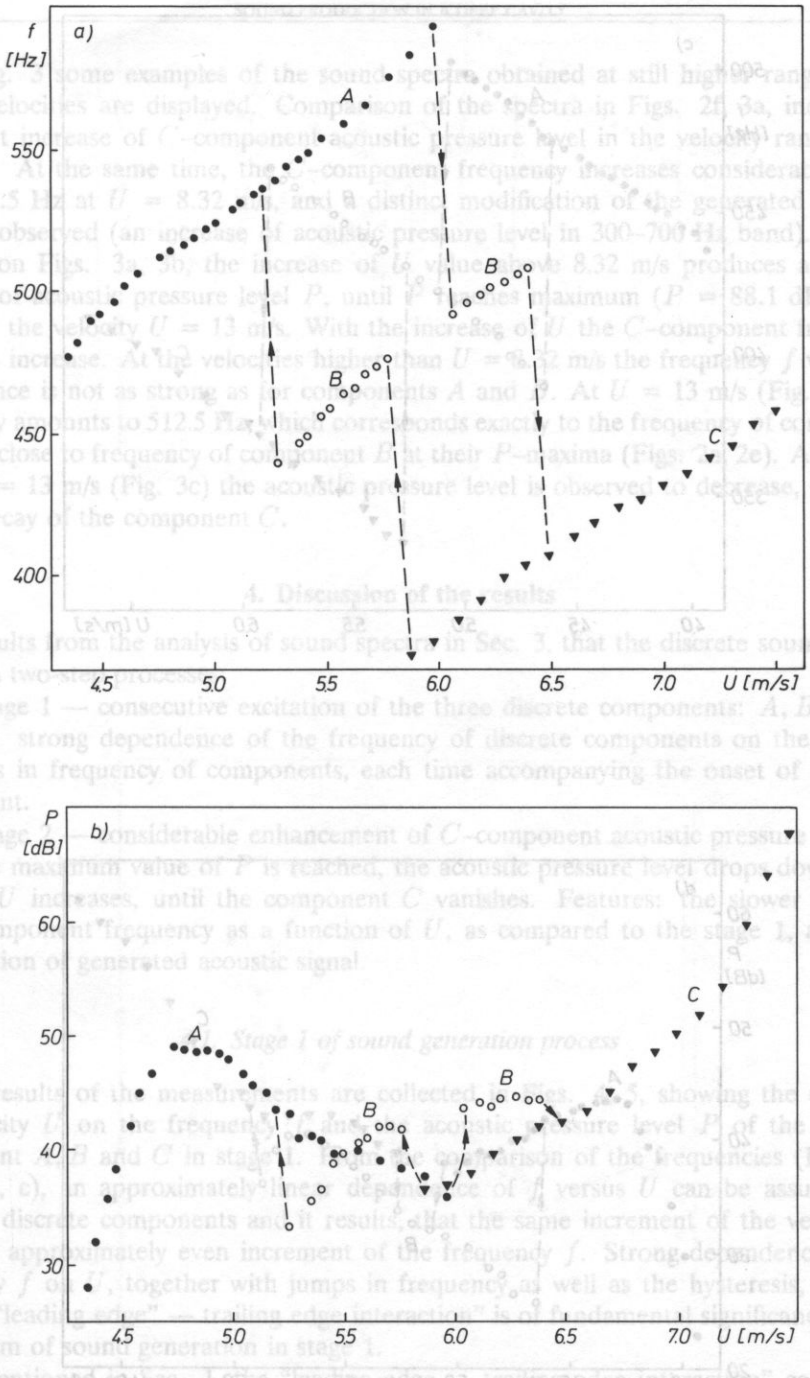

FIG. 4a,b. Frequency f and the acoustic pressure level P of the discrete components A, B and C in stage 1 of the sound generation process d = 12 cm.

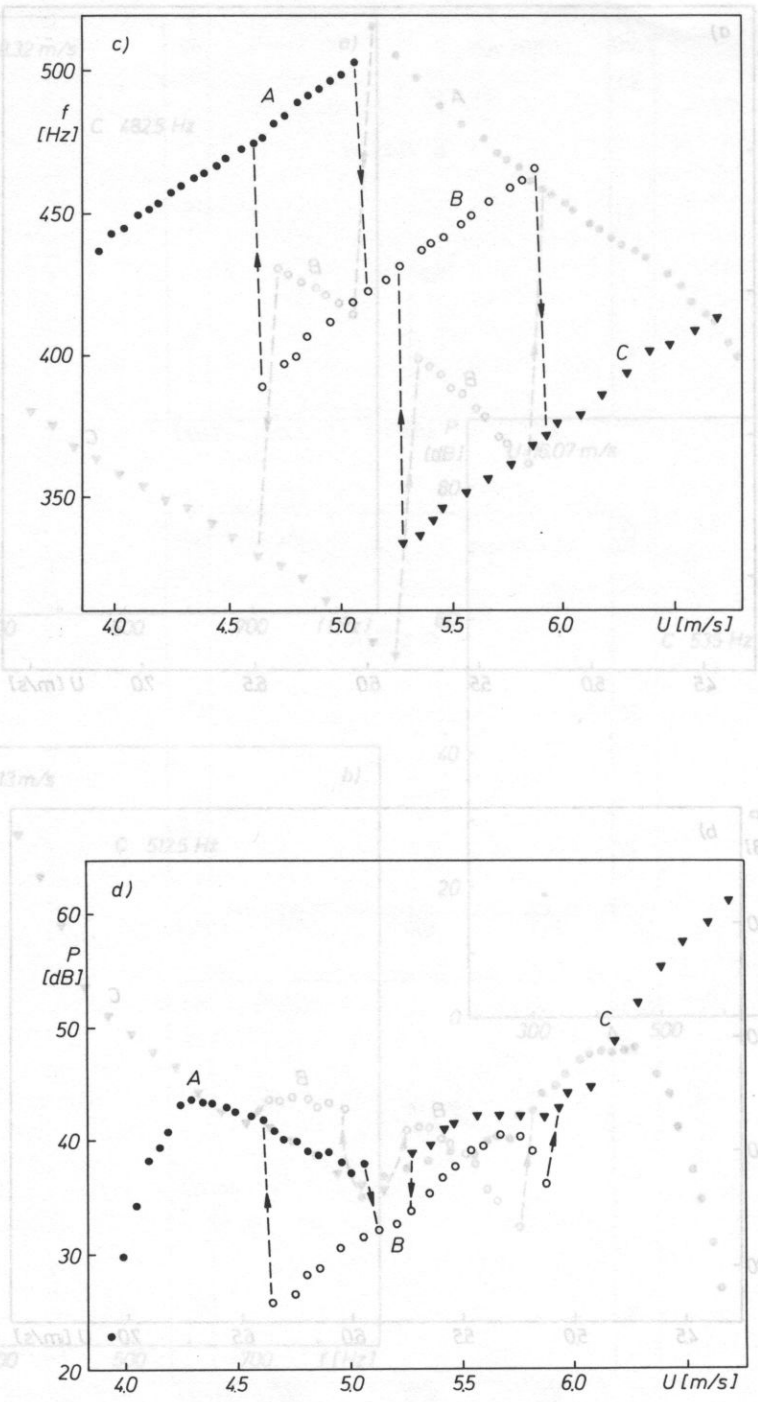

FIG. 4c,d. Frequency f and the acoustic pressure level P of the discrete components A, B and C in stage 1 of the sound generation process $d = 14$ cm.

In Fig. 3 some examples of the sound spectra obtained at still higher range of the airflow velocities are displayed. Comparison of the spectra in Figs. 2f, 3a, indicates a significant increase of C–component acoustic pressure level in the velocity range 6.48–8.32 m/s. At the same time, the C–component frequency increases considerably up to $f = 482.5$ Hz at $U = 8.32$ m/s, and a distinct modification of the generated acoustic signal is observed (an increase of acoustic pressure level in 300–700 Hz band). As can be seen on Figs. 3a, 3b, the increase of U value above 8.32 m/s produces a gradual increase of acoustic pressure level P, until P reaches maximum ($P = 88.1$ dB) which occurs at the velocity $U = 13$ m/s. With the increase of U the C–component frequency does also increase. At the velocities higher than $U = 8.32$ m/s the frequency f versus U dependence is not as strong as for components A and B. At $U = 13$ m/s (Fig. 3b) the frequency amounts to 512.5 Hz, which corresponds exactly to the frequency of component A and is close to frequency of component B at their P–maxima (Figs. 2a, 2e). Above the value $U = 13$ m/s (Fig. 3c) the acoustic pressure level is observed to decrease, followed by the decay of the component C.

4. Discussion of the results

It results from the analysis of sound spectra in Sec. 3, that the discrete sound generation is a two-step processes:

a) Stage 1 — consecutive excitation of the three discrete components: A, B and C. Features: strong dependence of the frequency of discrete components on the velocity U, jumps in frequency of components, each time accompanying the onset of the next component.

b) Stage 2 — considerable enhancement of C–component acoustic pressure level P. After the maximum value of P is reached, the acoustic pressure level drops down gradually as U increases, until the component C vanishes. Features: the slower increase of C–component frequency as a function of U, as compared to the stage 1, apparent modification of generated acoustic signal.

4.1. Stage 1 of sound generation process

The results of the measurements are collected in Figs. 4, 5, showing the effect of the velocity U on the frequency f and the acoustic pressure level P of the discrete component A, B and C in stage 1. From the comparison of the frequencies (Figs. 4a, c and 5a, c), an approximately linear dependence of f versus U can be assumed for all three discrete components and it results, that the same increment of the velocity U produces approximately even increment of the frequency f. Strong dependence of the frequency f on U, together with jumps in frequency as well as the hysteresis, indicate that the "leading edge" — trailing edge interaction" is of fundamental significance in the mechanism of sound generation in stage 1.

As mentioned in Sec. 1, the "leading edge — trailing edge interaction" constitutes one of two available mechanisms of the discrete sound generation by airflow over deep cavity. The main mechanism is based on the mutual interaction between shear layer disturbances and cavity-resonance modes (first-order flow-acoustic feedback). If in the process of sound generation, only this kind of feedback occurred, the frequency f of the

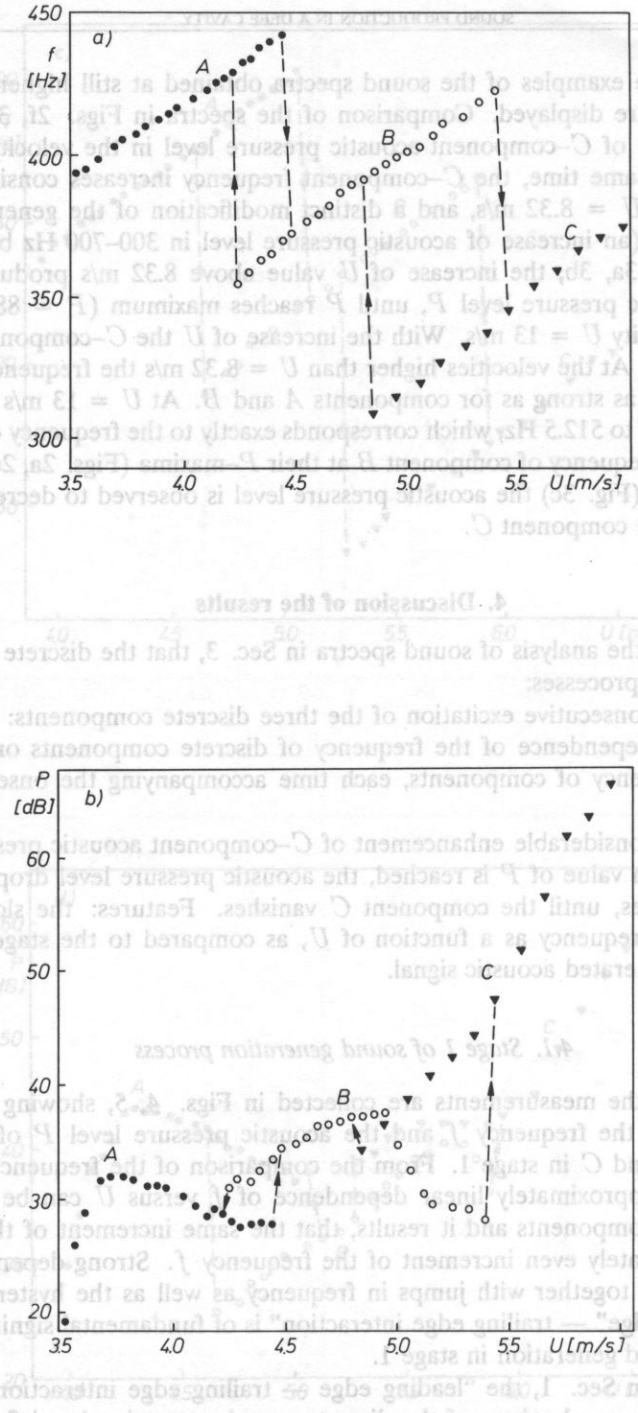

FIG. 5a,b. Frequency f and the acoustic pressure level P of the discrete components A, B and C in stage 1 of the sound generation process $d = 16$ cm.

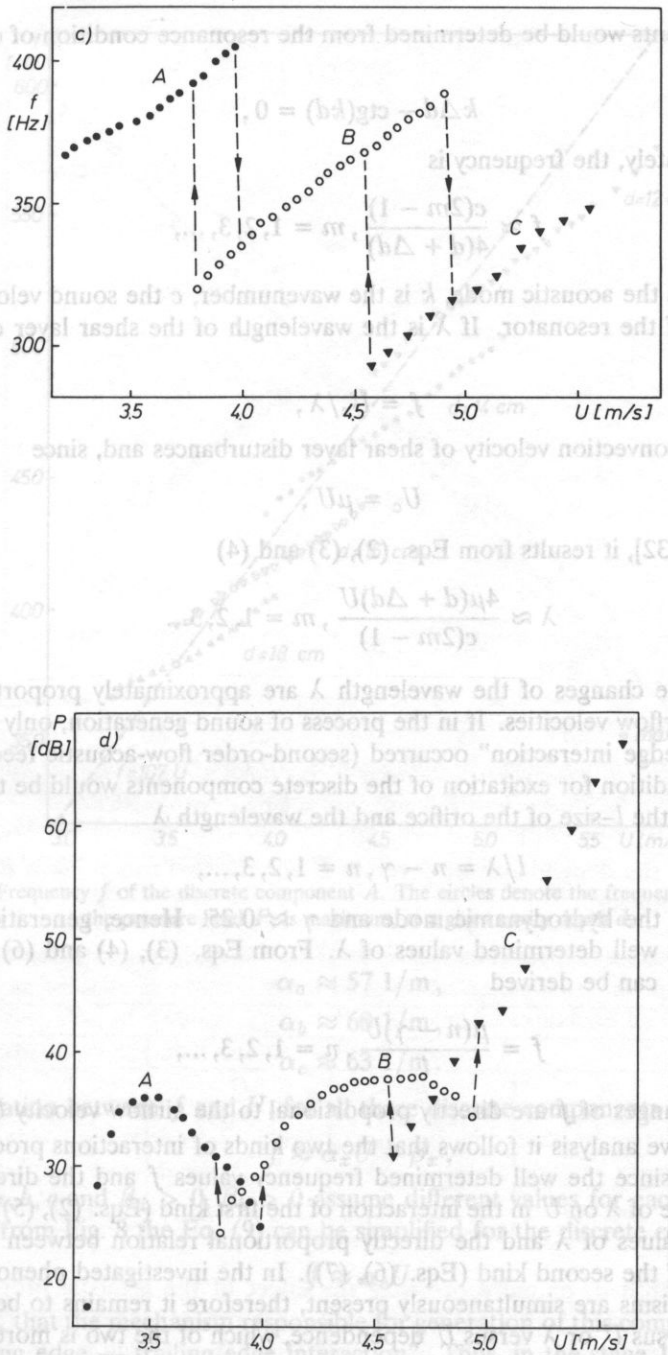

FIG. 5c,d. Frequency f and the acoustic pressure level P of the discrete components A, B and C in stage 1 of the sound generation process d = 18 cm.

discrete components would be determined from the resonance condition of quarter-wave resonator

$$k\Delta d - \operatorname{ctg}(kd) = 0\,, \tag{1}$$

hence, approximately, the frequency is

$$f \approx \frac{c(2m-1)}{4(d+\Delta d)}\,, m = 1,2,3,..., \tag{2}$$

where m denotes the acoustic mode, k is the wavenumber, c the sound velocity, Δd the end correction of the resonator. If λ is the wavelength of the shear layer disturbances, then

$$f = U_c/\lambda\,, \tag{3}$$

where U_c is the convection velocity of shear layer disturbances and, since

$$U_c = \mu U\,, \tag{4}$$

where $\mu \approx 0.62$ [32], it results from Eqs. (2), (3) and (4)

$$\lambda \approx \frac{4\mu(d+\Delta d)U}{c(2m-1)}\,, m = 1,2,3... \tag{5}$$

It means, that the changes of the wavelength λ are approximately proportional to the changes of the airflow velocities. If in the process of sound generation, only the "leading edge — trailing edge interaction" occurred (second-order flow-acoustic feedback), then the necessary condition for excitation of the discrete components would be the following relation between the l–size of the orifice and the wavelength λ

$$l/\lambda = n - \gamma\,, n = 1,2,3,..., \tag{6}$$

where n denotes the hydrodynamic mode and $\gamma \approx 0.25$. Hence, generation of sound can only occur at well determined values of λ. From Eqs. (3), (4) and (6) the relation between f and U can be derived

$$f = \frac{\mu(n-\gamma)U}{l}\,, n = 1,2,3,..., \tag{7}$$

therefore, the changes of f are directly proportional to the airflow velocity U.

From the above analysis it follows that the two kinds of interactions produce entirely opposite effects, since the well determined frequency values f and the directly proportional dependence of λ on U in the interaction of the first kind (Eqs. (2), (5)) correspond to the discrete values of λ and the directly proportional relation between f and U in the interaction of the second kind (Eqs. (6), (7)). In the investigated phenomenon both feedback mechanisms are simultaneously present, therefore it remains to be decided on the basis of f versus U or λ versus U dependence, which of the two is more important.

From the analysis of the data collected separately for the discrete component A, B and C (Figs. 6–8), conclusion can be reached that at each cavity depth d, the frequency f versus U dependence is similar. These dependencies can be characterized with $\Delta f/\Delta U$ ratios denoted α_a, α_b and α_c for the components A, B and C, respectively, amounting to

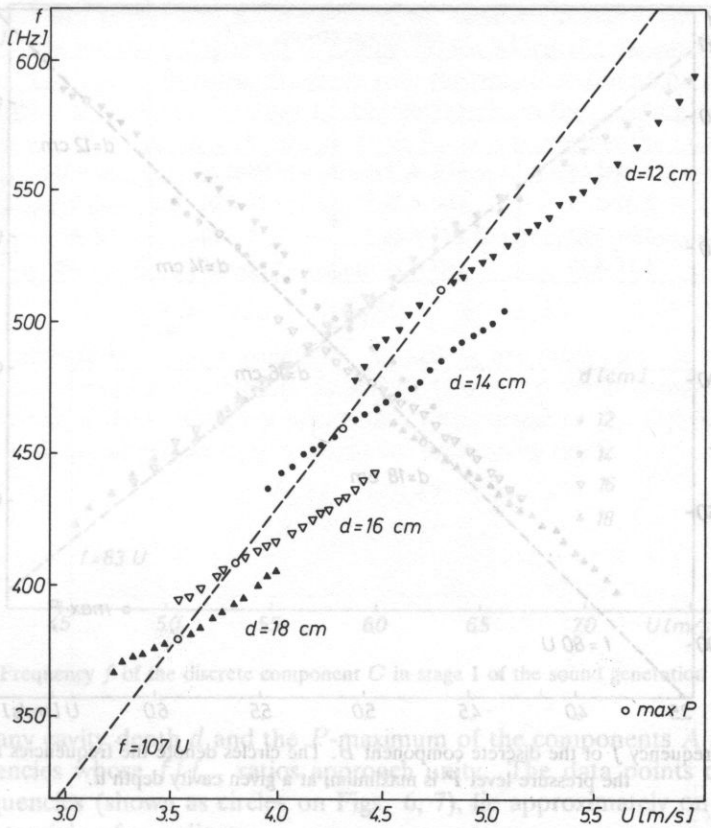

FIG. 6. Frequency f of the discrete component A. The circles denote the frequencies at which the pressure level P, is maximum, at a given cavity depth d.

$$\alpha_a \approx 57\ 1/\mathrm{m}, \quad \alpha_b \approx 60\ 1/\mathrm{m}, \quad \alpha_c \approx 63\ 1/\mathrm{m}. \tag{8}$$

Thus, the relation between f and U, for all three discrete components is

$$f \approx \alpha_x U + \beta_x, \tag{9}$$

where $x = a, b, c$ and $\beta_a > 0$, $\beta_b > 0$ assume different values for each cavity depth d. As it results from Fig. 8 the Eq. (9) can be simplified for the discrete component C

$$f \approx \alpha_c U \tag{10}$$

which means, that the mechanism responsible for generation of this component originates in the "leading edge — trailing edge interaction". Thus, in the stage 1, this component exhibits the character of the edgetone of the shear layer. Fast increase of f as a function of U, evident in the remaining two situations (Figs. 6, 7) shows that this kind of interaction is also of fundamental importance in producing the discrete components A and B. On the other hand, the fact that the values β_a and β_b in Eq. (9), are different from

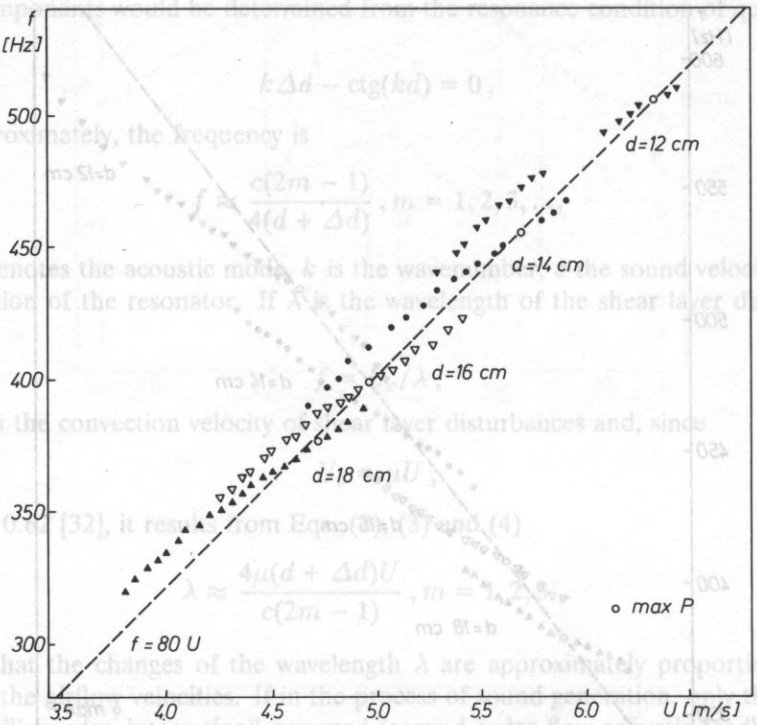

FIG. 7. Frequency f of the discrete component B. The circles denote the frequencies at which the pressure level P is maximum, at a given cavity depth d.

zero, means that the dependence of f versus U for the two components is modified by the first-order feedback.

Table 1. Frequencies ratios f/f_{res} of the discrete components A, B and C during stage 1 of the sound generation process

d [cm]	f/f_{res}				
	range			maximum P	
	A	B	C	A	B
12	0.93–1.16	0.86–1.00	0.73–0.90	1.000	0.985
14	0.96–1.10	0.85–1.02	0.73–0.91	1.005	0.995
16	0.98–1.10	0.88–1.05	0.77–0.93	1.012	0.991
18	0.97–1.07	0.85–1.03	0.76–0.92	1.003	0.997

The cavity depth d, or more precisely the effect of the acoustic properties of the resonator on the sound generation process, results in different frequency ranges at each value of d, as it can be seen in Figs. 6–8. Table 1 lists the limiting values of f/f_{res} ratio and the values of f/f_{res} corresponding to the maxima of acoustic pressure level P of the components A and B. The frequency f_{res} is that one at which the acoustic pressure level P of the component C, reaches the maximum value at a given cavity depth (Table 3). From these results it is evident that the range of f/f_{res} variations of each discrete component

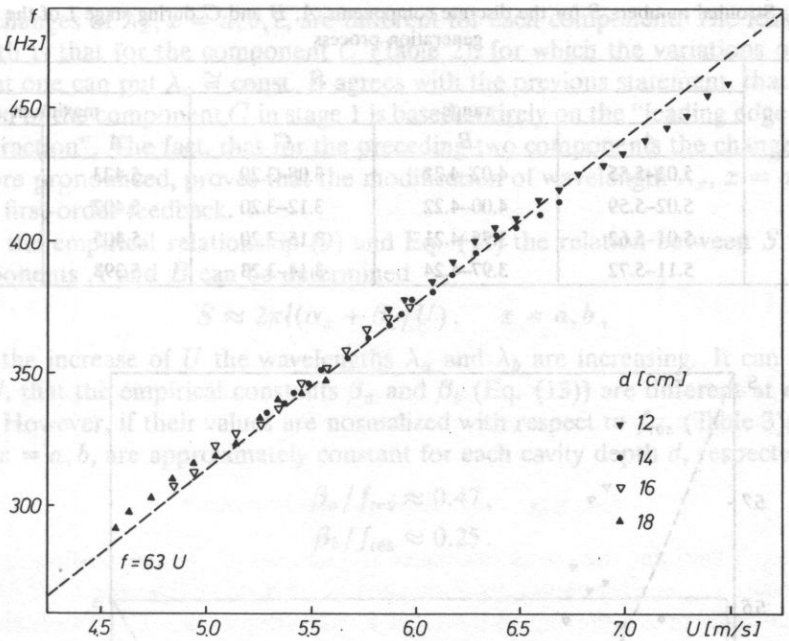

FIG. 8. Frequency f of the discrete component C in stage 1 of the sound generation process.

is similar at any cavity depth d and the P-maximum of the components A and B occurs at the frequencies whose f/f_{res} ratios approach unity. The data points corresponding to these frequencies (shown as circles on Figs. 6, 7), lie approximately on straight lines intersecting at origin of coordinates.

The effect of the acoustic properties of the resonator on the process of sound generation consists in the different, for each value of d, range of velocities U, in which a given discrete components occurs (Figs. 6–8). There is a correlation between the d and U variations, since the velocity at which a given component appears or vanishes, is observed to rise, with the decrease of d value. This correlation can be explained by the data collected in Table 2, where S is Strouhal number defined below

$$S = 2\pi f l/U\,. \tag{11}$$

One notices, that the range of S values, associated with each component, is practically independent of the cavity depth d. This rule has a simple physical meaning. Since, from Eqs. (3), (4) and (11)

$$\lambda = 2\pi\mu l/S\,, \tag{12}$$

therefore:

a) different wavelengths λ_a, λ_b and λ_c correspond to the three discrete components A, B and C,

b) $\lambda_a < \lambda_b < \lambda_c$,

c) quantity $\lambda_x, x = a, b, c$ assumes values within a precisely defined range.

Moreover, as it results from data in Table 2, $\lambda_a \cong$ const and $\lambda_b \cong$ const in the case of maximum P. Various sets of S values corresponding to each discrete component imply

Table 2. Strouhal numbers S for the discrete components A, B and C during stage 1 of the sound generation process

d [cm]	S				
	range			maximum P	
	A	B	C	A	B
12	5.01–5.55	4.02–4.21	3.08–3.20	5.423	4.042
14	5.02–5.59	4.00–4.22	3.12–3.20	5.402	4.034
16	5.01–5.62	3.95–4.21	3.15–3.20	5.405	4.049
18	5.11–5.72	3.97–4.24	3.14–3.23	5.393	4.025

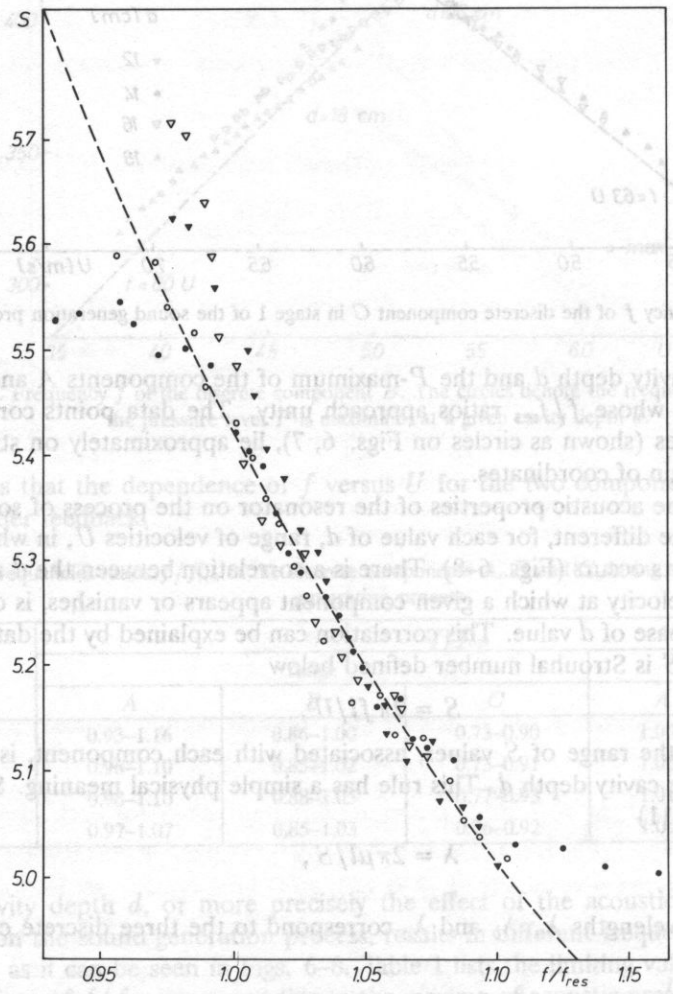

FIG. 9. The dependence of Strouhal number S on the f/f_{res} frequency ratio for the discrete component A: (●) d = 12 cm, (○) d = 14 cm, (▼) d = 16 cm, (▽) d = 18 cm, (- - -) S-values calculated from Eq. (16).

that the changes of $\lambda_x, x = a, b, c$, are different for each component. The least modified wavelength is that for the component C (Table 2), for which the variations of S are so small, that one can put $\lambda_c \cong$ const. It agrees with the previous statement, that the sound generation of the component C in stage 1 is based entirely on the "leading edge — trailing edge interaction". The fact, that for the preceding two components the changes of S are much more pronounced, proves that the modification of wavelength λ_x, $x = a, b$, results from the first-order feedback.

From the empirical relationship (9) and Eq. (11) the relation between S and U for the components A and B can be determined

$$S \approx 2\pi l(\alpha_x + \beta_x/U), \quad x = a, b, \tag{13}$$

i.e. with the increase of U the wavelengths λ_a and λ_b are increasing. It can be seen in Figs. 6, 7, that the empirical constants β_a and β_b (Eq. (13)) are different at each cavity depth d. However, if their values are normalized with respect to f_{res} (Table 3), the ratios $\beta_x/f_{\text{res}}, x = a, b$, are approximately constant for each cavity depth d, respectively

$$\begin{aligned} \beta_a/f_{\text{res}} &\approx 0.47, \\ \beta_b/f_{\text{res}} &\approx 0.25. \end{aligned} \tag{14}$$

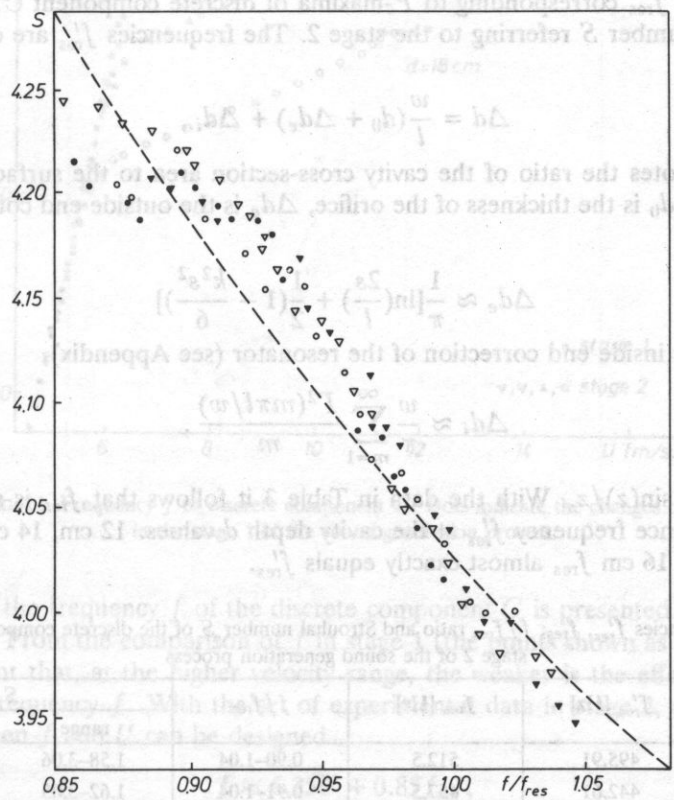

FIG. 10. The dependence of Strouhal number S on the frequency ratio f/f_{res} for the discrete component B: (•) d = 12 cm, (○) d = 14 cm, (▼) d = 16 cm, (▽) d = 18 cm, (- - -) S-values calculated from Eq. (17).

Equation (13) can be given in the alternative form

$$S \approx \frac{2\pi l \alpha_x}{1 - \beta_x / f}, \quad x = a, b, \tag{15}$$

hence, using Eqs. (8) and (14) one arrives at the expression for the component A

$$S \approx \frac{2.87}{f/f_{\text{res}} - 0.47}(f/f_{\text{res}}) \tag{16}$$

and

$$S \approx \frac{3.02}{f/f_{\text{res}} - 0.25}(f/f_{\text{res}}) \tag{17}$$

for the component B. It is evident from Figs. 9, 10 that S values calculated by the above two, equations agree with the experimental data.

4.2. Stage 2 of sound generation process

The Table 3 contains the cavity resonance frequencies f'_{res} under no-flow conditions, the frequencies f_{res} corresponding to P-maxima of discrete component C, f/f_{res} ratios and Strouhal number S referring to the stage 2. The frequencies f'_{res} are obtained from Eq. (1) with

$$\Delta d = \frac{w}{l}(d_0 + \Delta d_e) + \Delta d_i, \tag{18}$$

where w/l denotes the ratio of the cavity cross-section area to the surface area of the cavity opening, d_0 is the thickness of the orifice, Δd_e is the outside end correction of the resonator [22]

$$\Delta d_e \approx \frac{1}{\pi}[\ln(\frac{2s}{l}) + \frac{1}{2}(1 - \frac{k^2 s^2}{6})] \tag{19}$$

and Δd_i — the inside end correction of the resonator (see Appendix)

$$\Delta d_i \approx \frac{w}{\pi} \sum_{m=1}^{\infty} \frac{\Gamma^2(m\pi l/w)}{m}, \tag{20}$$

where $\Gamma(z) = \sin(z)/z$. With the data in Table 3 it follows that f_{res} is slightly higher than the resonance frequency f'_{res} at the cavity depth d values: 12 cm, 14 cm and 18 cm, whereas at $d = 16$ cm f_{res} almost exactly equals f'_{res}.

Table 3. Frequencies f'_{res}, f_{res}; f/f_{res} ratio and Strouhal number S of the discrete component C during stage 2 of the sound generation process

d [cm]	f'_{res} [Hz]	f_{res} [Hz]	f/f_{res}	S	
				range	max P
12	495.91	512.5	0.90–1.04	1.58–3.06	1.980
14	442.61	457.5	0.91–1.04	1.62–3.05	2.021
16	400.03	402.5	0.94–1.07	1.66–3.12	2.214
18	365.15	377.5	0.93–1.04	1.64–3.11	1.989

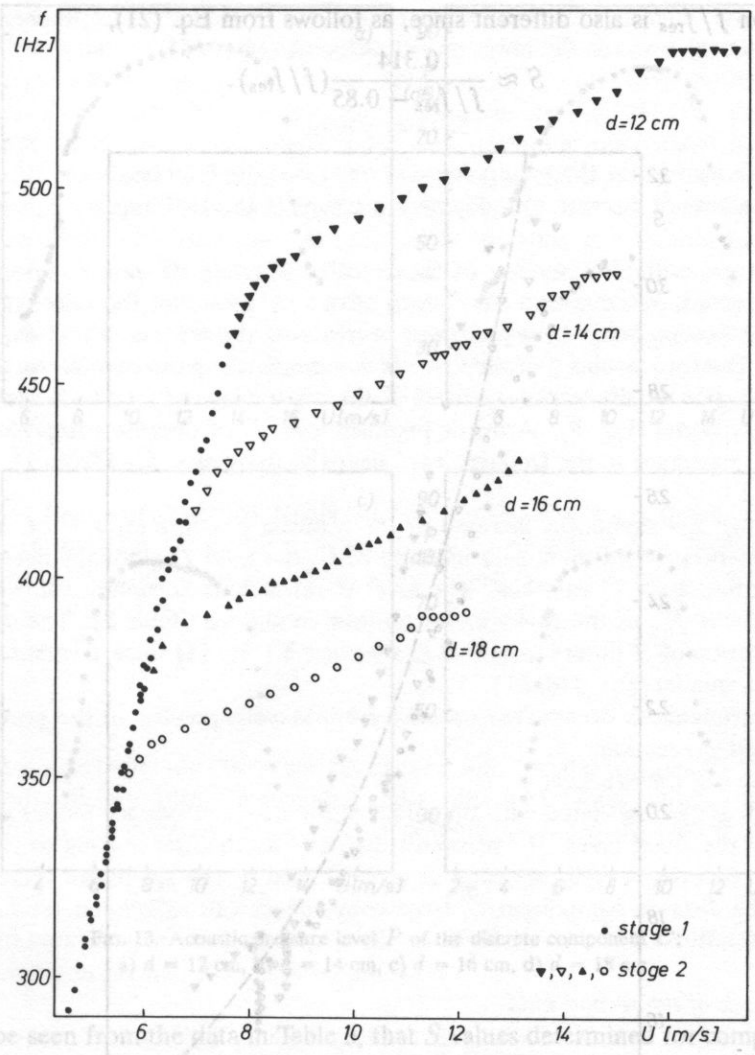

FIG. 11. Frequency f of discrete component C. Dots indicate the changes of f in the stage 1 of the sound generation process.

In Fig. 11 the frequency f of the discrete component C is presented as the function of velocity U. From the comparison of f in stage 1 (the points shown as dots) and stage 2 it is apparent that, at the higher velocity range, the weaker is the effect of the value of U on the frequency f. With the set of experimental data in stage 2, an approximate relation between f and U can be designed

$$f \approx 6.25U + 0.85 f_{\text{res}}, \tag{21}$$

Thus, the increase of f versus U is nearly ten times smaller than that in stage 1. Consequently, the range of f/f_{res} ratios is much smaller (Table 3). The dependence of Strouhal

number S on f/f_{res} is also different since, as follows from Eq. (21),

$$S \approx \frac{0.314}{f/f_{res} - 0.85}(f/f_{res}) . \tag{22}$$

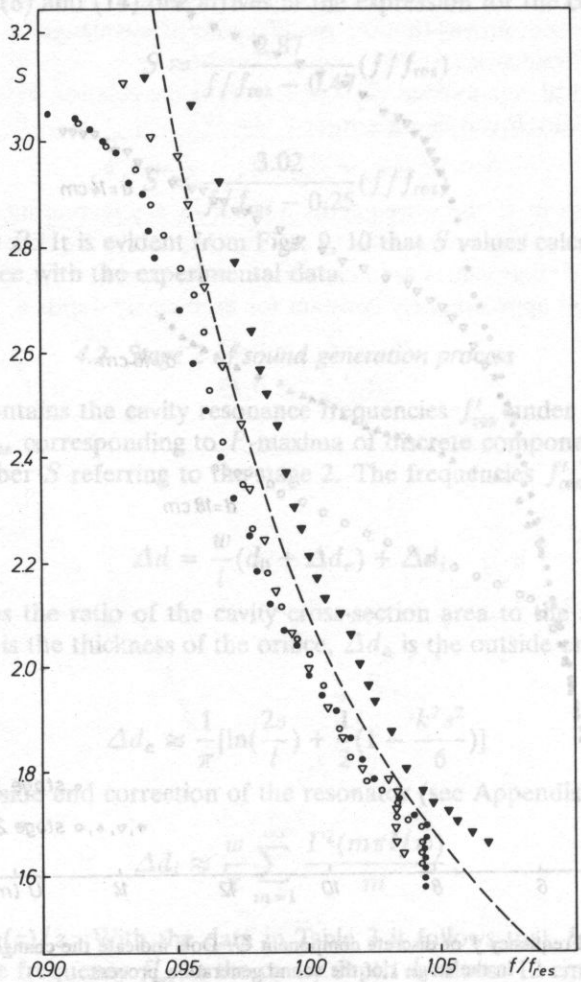

FIG. 12. The dependence of Strouhal number S on the frequency ratio f/f_{res} for the discrete component C in the stage 2 of the sound generation process: (•) d = 12 cm, (○) d = 14 cm, (▼) d = 16 cm, (▽) d = 18 cm, (- - -) S-values calculated from Eq. (22).

It results from the data in Table 3, that S range is very similar at all four values of the cavity depth d, thus the changes of λ_c are roughly independent of d. The fact that this range is much larger than that observed for the discrete components in stage 1 (Table 2), indicates that there is significant increase of λ_c value occurring at the higher stream velocities. According to our earlier conclusions, it proves a dominant role of the first-order feedback in stage 2.

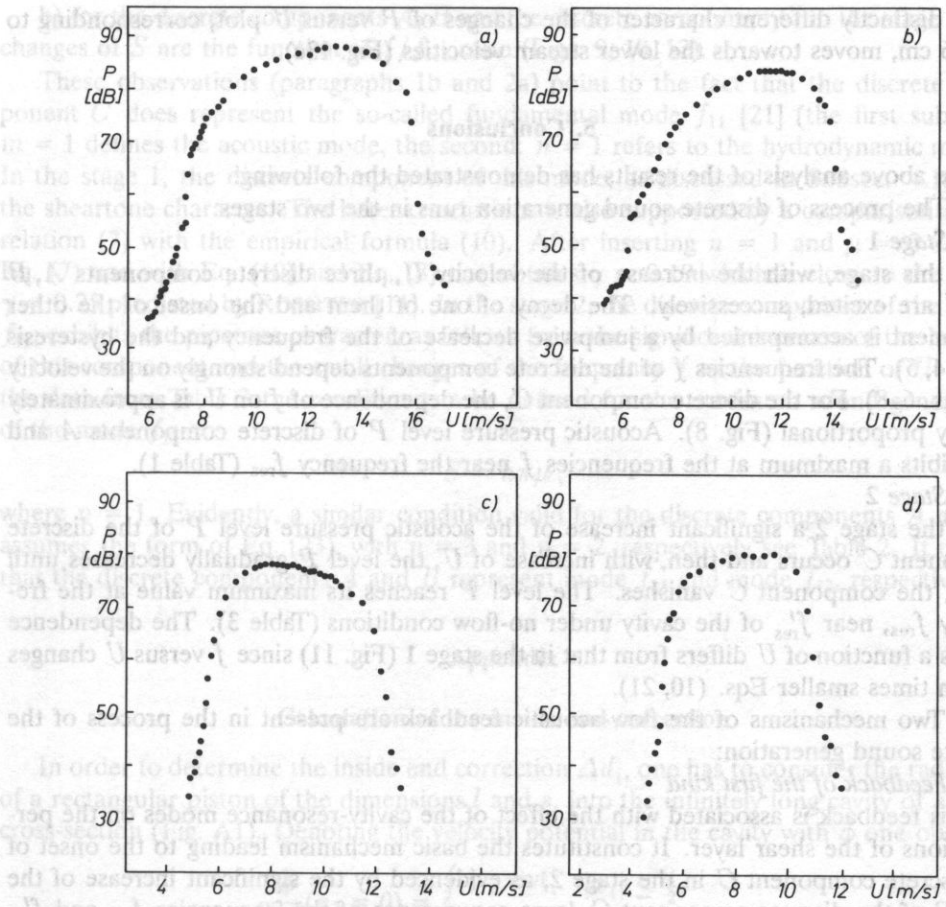

FIG. 13. Acoustic pressure level P of the discrete component C:
a) $d = 12$ cm, b) $d = 14$ cm, c) $d = 16$ cm, d) $d = 18$ cm.

It can be seen from the data in Table 3, that S values determined for component C at the maximum of P are observed to converge only at the cavity depth d equal 12 cm, 14 cm and 18 cm. Evidently larger value of S for the maximum of P ($S = 2.214$) and somewhat different range of f/f_{res} ratio observed for the cavity depth $d = 16$ cm, indicate that the measurement of the frequency f_{res} based on variation of P for the component C, may be in error. The extent to which this error affects the results of the measurement, can be seen in Fig. 12, where Strouhal number S has been plotted as a function of f/f_{res} ratio in stage 2. Large differences can be seen between the S values determined at the same f/f_{res} ratio, for the cavity depth $d = 16$ cm and for the remaining three values of d.

The error in the measurement of the frequency f_{res} is not due to a lack of precision of the method. For the cavity depth $d = 16$ cm the frequency and the acoustic pressure level can be measured accurately to 1.25 Hz and 0.1 dB, respectively (Sec. 2). On the other hand, the errors resulting from a main flow fluctuations, are eliminated by the averaging of spectra. The cause of the inaccuracy in the determination of f_{res} for $d = 16$ cm lies

in the distinctly different character of the changes of P versus U plot, corresponding to $d = 16$ cm, moves towards the lower stream velocities (Fig. 13c).

5. Conclusions

The above analysis of the results has demonstrated the following:

1) The process of discrete sound generation runs in the two stages:

a) *Stage* 1

In this stage, with the increase of the velocity U, three discrete components A, B and C are excited, successively. The decay of one of them and the onset of the other component is accompanied by a jumpwise decrease of the frequency and the hysteresis (Figs. 4, 5). The frequencies f of the discrete components depend strongly on the velocity U (Figs. 6–8). For the discrete component C, the dependence of f on U, is approximately directly proportional (Fig. 8). Acoustic pressure level P of discrete components A and B exhibits a maximum at the frequencies f near the frequency f_{res} (Table 1).

b) *Stage* 2

In the stage 2 a significant increase of the acoustic pressure level P of the discrete component C occurs and then, with increase of U, the level P gradually decreases until finally, the component C vanishes. The level P reaches its maximum value at the frequency f_{res}, near f'_{res} of the cavity under no-flow conditions (Table 3). The dependence of f as a function of U differs from that in the stage 1 (Fig. 11) since f versus U changes are ten times smaller Eqs. (10, 21).

2) Two mechanisms of the flow-acoustic feedback are present in the process of the discrete sound generation:

a) *Feedback of the first kind*

This feedback is associated with the effect of the cavity-resonance modes on the perturbations of the shear layer. It constitutes the basic mechanism leading to the onset of the discrete component C in the stage 2, as evidenced by the significant increase of the level P of the discrete component C, large convergence of the frequencies f_{res} and f'_{res} and the small influence of the velocity U on the frequency f of the generated sound (Figs. 11, 13).

b) *Feedback of the second kind*

This feedback is associated with the "leading edge — trailing edge interaction", i.e. the effect of the acoustic perturbations, occurring at the leading edge of the cavity orifice, on the shear layer disturbances at the trailing edge. This kind of coupling is decisive in the generation of the discrete components A and B as well as the discrete component C in the stage 1. It has been evidenced by the strong dependence of the frequency f on the velocity U, the jumpwise changes of f occurring at the excitation of successive discrete components and by hysteresis (Figs. 4, 5).

3) Three different wavelengths: $\lambda_a < \lambda_b < \lambda_c$ refer to the discrete components A, B and C, correspondingly. The range of λ_x values, with $x = a, b, c$ is strinctly defined, as evidenced from the similar ranges of Strouhal number S, obtained for each component at the various depths d of cavity (Tables 2, 3).

4) The modification of the wavelength $\lambda_x, x = a, b, c$, is the result of the feedback of the first kind. This conclusion is supported by the following observations:

a) the largest range of S values occurs in the stage 2 (Table 3),

b) for the discrete components A, B and the discrete component C in the stage 2, the changes of S are the function of f/f_{res} ratio (Figs. 9, 10, 12).

These observations (paragraphs 1b and 2a) point to the fact that the discrete component C does represent the so-called fundamental mode f_{11} [21] (the first subscript $m = 1$ defines the acoustic mode, the second: $n = 1$ refers to the hydrodynamic mode). In the stage 1, the discrete component of this mode, as discussed in Subsec. 4.1, is of the sheartone character. The latter conclusions is also supported by a comparison of the relation (7) with the empirical formula (10). After inserting $n = 1$ and $\mu = 0.62$ into Eq. (7) and with Eq. (10) and Eq. (8) one obtains $\gamma = 0.19$ which is close to the value $\gamma = 0.25$ predicted by ROSSITER [11]. In the stage 2, the discrete component of the mode f_{11}, exhibits the pipetone character, as follows from the significant increase of the level P of this component and the small changes of the frequency f as the function of U. With the data from Table 3 the condition can be defined for the maximum sound generation of the mode f_{11}

$$S = n\pi\mu\,, \tag{23}$$

where $n = 1$. Evidently, a similar condition valid for the discrete components A and B assumes the form of Eq. (23), with $n = 3$ and $n = 2$, respectively see Table 2. It means that the discrete components A and B represent mode f_{13} and mode f_{12}, respectively.

Appendix

Calculation of the inside end correction

In order to determine the inside end correction Δd_i, one has to consider the radiation of a rectangular piston of the dimensions l and s, into the infinitely long cavity of s by w cross-section (Fig. A1). Denoting the velocity potential in the cavity with ϕ one obtain

$$\frac{\partial\phi}{\partial x_2}(x_2 = 0) = \begin{cases} Ve^{-j\omega t}, & |x_1| \leq \frac{l}{2}, \\ 0, & \frac{l}{2} < |x_1| \leq \frac{w}{2}. \end{cases} \tag{A1}$$

From the condition A1 and Fig. A1 it results, that

$$\phi = Ve^{-j\omega t} \int_{-\frac{s}{2}}^{\frac{s}{2}} \int_{-\frac{l}{2}}^{\frac{l}{2}} G(\overline{x}, \overline{y}) dy_1 dy_3\,, \tag{A2}$$

where $\overline{x} = (x_1, x_2, x_3)$, $\overline{y} = (y_1, 0, y_3)$ and Green's function G is the solution of the following equation

$$\nabla^2 G + k^2 G = -\delta(x_1 - y_1)\delta(x_2)\delta(x_3 - y_3)\,, \tag{A3}$$

and fulfills the boundary conditions

$$\frac{\partial G}{\partial x_1}\left(x_1 = -\frac{w}{2}\right) = \frac{\partial G}{\partial x_1}\left(x_1 = \frac{w}{2}\right) = 0\,, \tag{A4}$$

$$\frac{\partial G}{\partial x_3}\left(x_3 = -\frac{s}{2}\right) = \frac{\partial G}{\partial x_3}\left(x_3 = \frac{s}{2}\right) = 0\,. \tag{A5}$$

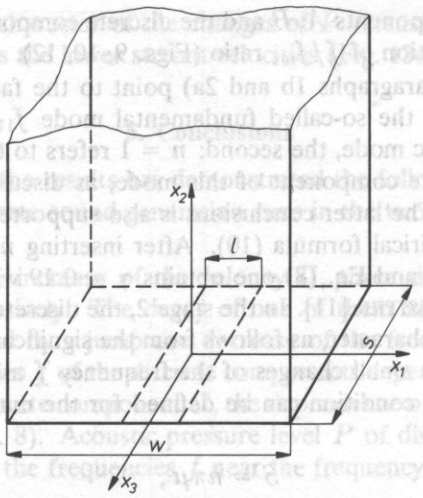

FIG. A1. Rectangular piston dimension l and s situated in the infinitely long channel wall and cross-section s by w.

Finally, the solution to Eq. (A3), under the boundary conditions (A1), (A4) and (A5), is the function G

$$G(\overline{x}, \overline{y}) = \frac{j}{sw} \sum_{m=0}^{\infty} \sum_{n=0}^{\infty} \frac{\epsilon_m \epsilon_n \psi_{mn}(x_1, x_3) \psi_{mn}(y_1, y_3)}{k_{mn}} e^{jk_{mn}x_2}, \tag{A6}$$

where ϵ_m and ϵ_n is Neumann factor

$$\psi_{mn}(z_1, z_3) = \cos(2m\pi z_1/w)\cos(2n\pi z_3/s),$$
$$k_{mn} = [k^2 - (2m\pi/w)^2 - (2n\pi/s)^2]^{1/2}.$$

The reactive force of the medium due to vibrations of the piston in the cavity opening can be determined from the formula

$$F = |F|e^{-j\omega t} = -\int_{-\frac{s}{2}}^{\frac{s}{2}} \int_{-\frac{l}{2}}^{\frac{l}{2}} p(x_2 = 0) dx_1 dx_3, \tag{A7}$$

where $p(x_2 = 0)$ is the pressure acting upon the piston

$$p(x_2 = 0) = j\omega\varrho\phi(x_2 = 0), \tag{A8}$$

hence, after substituting (A8) in (A7), using (A2) and (A6) and integrating, one obtains

$$|F| = l^2 s^2 V \left[\frac{\varrho c}{sw} + \frac{2\varrho\omega}{sw} \sum_{m=1}^{\infty} \frac{\Gamma^2(m\pi l/w)}{k_m}\right], \tag{A9}$$

where $\Gamma(z) = \dfrac{\sin(z)}{z}$ and $k_m = [k^2 - (2m\pi/w)]^{1/2}$. In the case of the frequency ω much lower than the higher modes frequencies of the cavity

$$k_m \approx 2jm\pi/w, \tag{A10}$$

therefore, from (A9)

$$\frac{|F|}{l^2 s^2 V} \approx \frac{\varrho c}{sw} - \frac{j\varrho\omega}{sw}\left[\frac{w}{\pi}\sum_{m=1}^{\infty}\frac{\Gamma^2(m\pi l/w)}{m}\right]. \tag{A11}$$

The first term of the right hand side of the Eq. (A1) is the wave impedance of the cavity (plane wave impedance), whereas the second term represents the impedance of the acoustic inertance M of the co-vibrating medium

$$M = \frac{\varrho}{sw}\Delta d_i\,, \tag{A12}$$

thus

$$\Delta d_i \approx \frac{w}{\pi}\sum_{m=1}^{\infty}\frac{\Gamma^2(m\pi l/w)}{m}\,. \tag{A13}$$

References

[1] L. Cremer, H. Ising, *Die selbsterregten Schwingungen von Orgelpfeifen*, Acustica, **19**, 143–153 (1967/68).

[2] J. W. Coltman, *Sounding mechanism of sound production in organ pipes*, J. Acoust. Soc. Am. **44**, 983–992 (1968).

[3] N. H. Fletcher, *Sound production by organ flue pipes*, J. Acoust. Soc. Am. **60**, 4, 926–936 (1976).

[4] J. L. King, P. Boyle, J. B. Ogle, *Instability in slotted wall tunnels*, J. Fluid Mech. **4**, 283–305 (1958).

[5] G. F. McCanless, J. R. Boone, *Noise reduction in transonic wind tunnels*, J. Acoust. Soc. Am. **56**, 5, 1501–1510 (1974).

[6] J. C. Bruggeman, *Flow induced pulsations in pipe systems*, Ph.D. thesis, Eindhoven, 1987.

[7] C. K. Tam, P. J. Block, *On the tones and pressure oscillations induced by flow over rectangular cavities*, J. Fluid Mech. **89**, 373–399 (1978).

[8] W. L. Hankey, J. S. Shang, *Analyses of pressure oscillations in an open cavity*, AIAA J. **18**, 8, 892–898 (1980).

[9] D. Rockwell, E. Naudascher, *Review — self-sustaining oscillations of flow past cavities*, J. Fluids Engineering, Trans. ASME **100**, 152–165 (1978).

[10] D. Rockwell, *Oscillations of impinging shear layers*, AIAA J. **21**, 5, 645–664 (1983).

[11] J. E. Rossiter, *Wind tunnel experiments on the flow over rectangular cavities at subsonic and transonic speeds*, RAE Report No. 64037 (1964).

[12] H. H. Heller, D. G. Holmes, E. E. Covert, *Flow-induced pressure oscillations in shallow cavities*, J. Sound Vib. **18**, 4, 545–553 (1971).

[13] A. J. Bilanin, E. E. Covert, *Estimation of possible excitation frequencies for shallow rectangular cavities*, AIAA J. **11**, 3, 347–351 (1973).

[14] V. Sarohia, *Experimental investigation of oscillations in flow over shallow cavities*, AIAA J. **15**, 7, 984–991 (1977).

[15] L. F. East, *Aerodynamically induced resonance in rectangular cavities*, J. Sound Vib. **3**, 3, 277–287 (1966).

[16] E. E. Covert, *An approximate calculation of the onset velocity of cavity oscillations*, AIAA J. **8**, 12, 2189–2194 (1970).

[17] S. A. Elder, *Self-excited depth-mode resonance for wall-mounted cavity in turbulent flow*, J. Acoust. Soc. Am. **64**, 3, 877–890 (1978).

[18] S. A. Elder, *Forced oscillations of separated shear layer with application to cavity flow-tone effects*, J. Acoust. Soc. Am. **67**, 3, 774–781 (1980).

[19] M. L. Pollack, *Flow-induced tones in side-branch pipe resonators*, J. Acoust. Soc. Am. **67**, 4, 1153–1156 (1980).

[20] M. S. Howe, *The influence of mean shear on unsteady aperture flow, with application to acoustical diffraction and self-sustained oscillations*, J. Fluid Mech. **109**, 125–146 (1981).

[21] S. A. ELDER, T. M. FARABEE, F. C. DEMETZ, *Mechanisms of flow-excited tones at low Mach number*, J. Acoust. Soc. Am. **72**, 2, 532–549 (1982).
[22] M. MEISSNER, *Self-sustained deep cavity oscillations induced by grazing flow*, Acustica, **62**, 3, 220–228 (1987).
[23] R. L. PANTON, J. M. MILLER, *Excitation of a Helmholtz resonator by turbulent boundary layer*, J. Acoust. Soc. Am. **58**, 4, 800–806 (1975).
[24] J. S. ANDERSON, *The effect of an air flow on a single side branch Helmholtz resonator in a circular duct*, J. Sound Vib. **52**, 3, 423–431 (1977).
[25] P. A. NELSON, N. A. HALLIWELL, P. E. DOAK, *Fluid dynamics of a flow excited resonance, Part* I: *Experiment*, J. Sound Vib. **78**, 1, 15–38 (1981).
[26] P. A. NELSON, N. A. HALLIWELL, P. E. DOAK, *Fluid dynamics of a flow excited resonance, Part* II: *Flow acoustic interaction*, J. Sound Vib. **91**, 3, 375–402 (1983).
[27] M. MÖSER, *Aktive Kontrolle einfacher, selbsterregter Resonatoren*, Acustica, **69**, 4, 175–184 (1989).
[28] F. C. DEMETZ, T. M. FARABEE, *Laminar and turbulent shear flow induced resonances*, AIAA paper 77–1293 (1977).
[29] A. POWELL, *On the edgetone*, J. Acoust. Soc. Am. **33**, 4, 395–409 (1961).
[30] D. K. HOLGER, T. A. WILSON, G. S. BEAVERS, *Fluid dynamics of the edgetone*, J. Acoust. Soc. Am. **62**, 5, 1116–1128 (1977).
[31] S. OHRING, *Calculation of self-excited impinging jet flow*, J. Fluid Mech. **163**, 69–98 (1986).
[32] M. E. GOLDSTEIN, *Aeroacoustics*, Mc Graw-Hill, New York 1976, p. 91.

Received on August 30, 1990; English version April 15, 1992